Front. Phys. 11(2), 117301 (2016)
DOI 10.1007/s11467-015-0524-7

REVIEW ARTICLE

Deviating from the nanorod shape: Shape-dependent plasmonic properties of silver nanorice and nanocarrot structures

Hong-Yan Liang[1], Hong Wei[2], Hong-Xing Xu[1,†]

[1] *Center for Nanoscience and Nanotechnology, School of Physics and Technology, and Institute for Advanced Studies, Wuhan University, Wuhan 430072, China*

[2] *Institute of Physics, Chinese Academy of Sciences, and Beijing National Laboratory for Condensed Matter Physics, Beijing 100190, China*

Corresponding author. E-mail: †hxxu@whu.edu.cn

Received July 12, 2015; accepted October 26, 2015

Noble metallic nanostructures exhibit special optical properties resulting from excitation of surface plasmons. Among the various metallic nanostructures, nanorods have attracted particular attention because of their unique and intriguing shape-dependent plasmonic properties. Nanorods can support transverse and longitudinal plasmon modes, the latter ones depending strongly on the aspect ratio of the nanorod. These modes can be routinely tuned from the visible to the near-infrared spectral regions. Although nanorods have been investigated extensively, there are few studies devoted to nanostructures deviating from the nanorod shape. This review provides an overview of recent progress in the development of two kinds of novel quasi-one-dimensional silver nanostructures, nanorice and nanocarrot, including their syntheses, crystalline characterizations, plasmonic property analyses, and performance in plasmonic sensing applications.

Keywords electron energy loss spectroscopy (EELS), localized surface plasmon resonance (LSPR), multipolar longitudinal plasmon mode, nanocarrot, nanorice, plasmonic sensing

PACS numbers 73.20.Mf, 78.67.Qa, 61.46.Df, 81.16.Be

Contents

1 Introduction

Noble metallic nanostructures have drawn considerable attention due to their unique plasmonic characteristics and good performance in a variety of applications [1–5]. When the frequency of incident electromagnetic radiation matches the natural oscillation frequency of the conduction electrons on the surface of metallic nanostructures, strong localized surface plasmon resonances (LSPRs) occur. LSPRs produce large local electric field at the metal-dielectric interface, and dramatically increase light scattering and absorption [1]. In addition, LSPRs are very sensitive to changes in the surrounding media. When the dielectric environment changes, the frequencies of LSPRs shift accordingly [6]. These properties of LSPRs in metallic nanostructures have been applied to surface-enhanced Raman spectroscopy (SERS) [7–18], chemical and biochemical sensing [6, 19, 20], optical trapping [21–23], and nano-antennas [24–26]. It is well known that the energy of LSPRs in metallic nanostructures is determined by their compositions, dimensions, and geometries, which influence the electron density on the nanostructure surface. By controlling the size and shape of a nanostructure, the wavelength of a LSPR can be tuned accordingly. This characteristic is critical for practical applications occurring at different wavelengths.

*Special Topic: Frontiers of Plasmonics (Ed. Hong-Xing Xu).

Nanorods, which have a remarkable ability to tune LSPRs, have attracted a lot of interest [27–34]. Spherical nanoparticles usually display only one degenerate dipolar LSPR mode with an intensity maximum generally centered in the visible light region [35]. Nanorods, however, display two types of distinct LSPRs, which are transverse modes corresponding to the short axis resonances, and longitudinal modes corresponding to the long axis resonances [27–29]. While the energy of transverse LSPRs in nanorods is relatively insensitive to size changes, the energy of longitudinal LSPRs depends linearly on the aspect ratio of the nanorod [28, 29]. By manipulating the aspect ratio, the wavelengths of longitudinal LSPRs can be tuned from the visible region of the electromagnetic spectrum to the near-infrared region, allowing nanorods to be used for many more applications. As the aspect ratio increases, high-order longitudinal LSPRs appear that are analogous to Fabry–Pérot (FP) resonances along the long axis resulting from the reflections of surface plasmons at two terminals [27–29, 36]. Compared with the longitudinal dipole mode, the multipolar LSPRs possess lower energy losses and higher quality factors [29]. The longitudinal modes in nanorods are ultrasensitive to any change in the dielectric constant of the surrounding medium, which makes nanorods excellent LSPR sensors [37, 38]. In view of such advantages in plasmonic applications, nanorods have been studied extensively in recent years.

When the shape of metallic nanostructure deviates from a nanorod shape, the optical properties are affected. There are few studies on deformed nanorod shapes due to difficulties in experimental synthesis, and the analyses of the corresponding plasmonic properties are insufficient. Aimed at tailoring plasmonic features and improving performance in different applications, we have synthesized and investigated two types of quasi-one-dimensional plasmonic nanostructures: silver nanorice [39] and silver nanocarrot [40]. These two novel nanostructures provide an opportunity for researchers to experimentally study the plasmonic properties of deformed nanorod structures and their advantages in applications. In this review, we will provide an overview of the synthesis, crystalline structure characterization, plasmonic property analysis, and applications of nanorice and nanocarrot structures. Their shape-dependent optical properties, such as high-order plasmon modes and plasmonic Fano resonances, are introduced and discussed in detail. Their potential for applications in sensing and surface-enhanced spectroscopy is discussed as well.

2 Silver nanorice structures

2.1 Synthesis and structure characterization

Nanorods have a constant diameter, which is usually modeled by a right circular cylinder with either flat or hemispherical ends. When the diameter of this cylinder decreases gradually from the center to the two ends, it forms nanorice in a prolate spheroid shape. Large-scale and high-yield preparation of silver nanorice structures with a uniform shape through a facile polyol route was reported by Liang *et al.* [39]. In a typical synthesis, 0.5 mL of 1 M aqueous $AgNO_3$ and 2.5 mL of 1 M aqueous poly (vinyl pyrrolidone) (PVP, Mw $\approx$ 40 000, the concentration was calculated in terms of the repeating unit) were dissolved in 25 mL poly (ethylene glycol) 600 (PEG 600) in a flask with stirring. The flask was placed in an oil bath and heated at 100 °C for ~8 h. A gray silver colloid resulted. In this synthesis, PVP acts as a stabilizer, and PEG 600 acts as both solvent and reducing agent. The crystalline structure of the silver nanorice was studied by both powder X-ray diffraction (XRD) and transmission electron microscopy (TEM) with electron diffraction (ED). The nanorice structure has a nearly smooth surface and round ends, as shown in Fig. 1(a). Except for the typical FCC phase, which generally exists in silver nanostructures, the HCP phase also appears in the nanorice structure, as indicated by the XRD pattern in Fig. 1(b). This HCP phase was confirmed by high-resolution TEM (HRTEM) images in Fig. 1(c), and the ED pattern in Fig. 1(d). Unlike conventional silver nanostructures that have a single or five-fold twinning structure, silver nanorice consist of the intergrowth of a series of stacking faults, as indicated by the black arrows in Fig. 1(c) (i), and nanoscale twinning structures from the FCC phase, as indicated by dashed lines in Fig. 1(c) (ii), and a small amount of HCP phase, as labeled by "Hexagonal" in Fig. 1(c) (i). The increasing density of stacking faults and HCP phase along the $\langle 111 \rangle$ growth direction towards the end may reduce the surface energy, which determines the prolate contour of the nanorice [39].

To shed light on the growth kinetics of the silver nanorice under our synthesis conditions, the growth process was followed by taking out aliquots of reaction solution at certain time intervals, and observing their color [41]. At the onset of the reaction, the solution showed a light yellow color, which faded gradually after heating. Then, the light yellow color reappeared and turned into green. The green color intensified as the reaction proceeded. All of the intermediate reaction solutions were analyzed by ultraviolet–visible–near-infrared (UV-Vis-

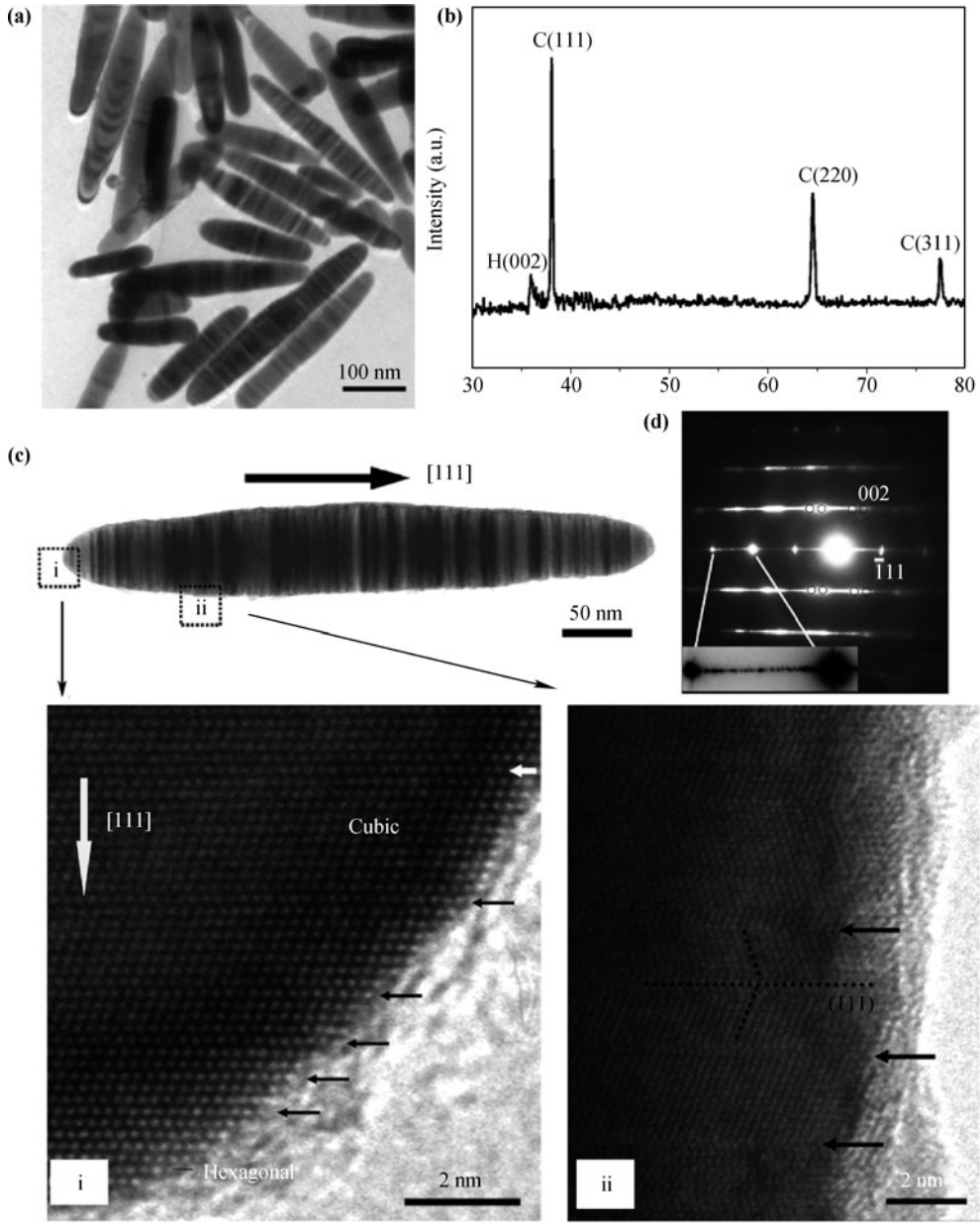

Fig. 1 **(a)** TEM image of silver nanorice. **(b)** XRD pattern from the same batch of sample used in (a). **(c)** Low-magnification TEM image of a typical nanorice and HRTEM images for the square-enclosed regions. **(d)** The ED pattern corresponding to (c). Reproduced from Ref. [39].

NIR) spectroscopy and TEM. Based on the experimental observations, a basic growth mechanism was proposed for the silver nanoparticles that evolved from a spherical shape to a rice shape, as illustrated in Fig. 2(a). At the beginning, silver ions are reduced to form silver nanoparticles, which contribute to the light yellow color of the solution. As the reaction continues, oxygen dissolved in the PEG 600 solution selectively etches the twinning silver nanoparticles because they have higher chemical reactivity. The reduction of the twinning nanoparticles leads to color fading of the solution. At the same time, the small-size single crystals with lower chemical reactivity remain intact, growing into primary nanoparticles through Oswald ripening. Hence, the light yellow color reappears. Then, the larger-size primary nanoparticles make contact with each other by an oriented attached way to form intermediate quasi-one-dimensional nanostructures [shown in Fig. 2(b)]. These nanostructures produce the green solution color. Eventually, they evolve into typical nanorice structures via continuous oriented attachment fed by oxygen-etching selected seeds, combined with lateral growth fed by atomic diffusion [41].

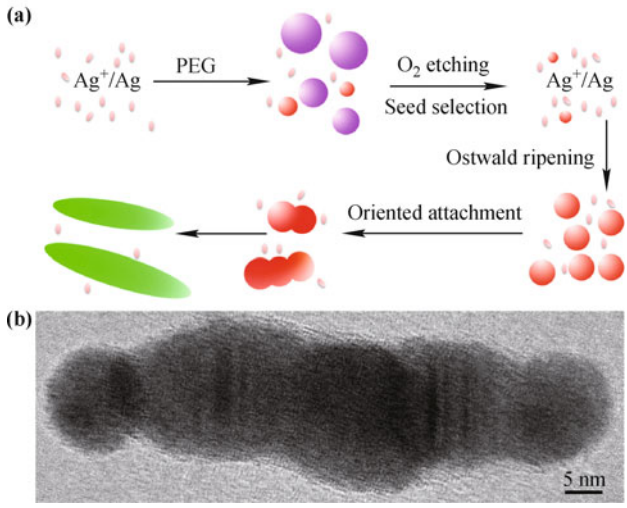

Fig. 2 **(a)** Proposed growth process of silver nanorice structures (pink: Ag^0 or Ag^+; red: Single crystal; purple: Twinned crystal; green: Nanorice). **(b)** TEM image showing the oriented attachment of silver nanoparticles. Reproduced from Ref. [41].

2.2 Plasmonic properties of nanorice structures

The extinction spectrum of an ensemble of silver nanorice structures, shown in the scanning electron microscopy (SEM) image [Fig. 3(a)] was measured in an ethanol suspension [Fig. 3(b)] [42]. Due to the prolate shape, the spectrum is characterized by transverse and longitudinal plasmon resonances. It is important to point out that multipolar longitudinal LSPRs appear in the extinction spectrum, as marked in Fig. 3(b), which were further characterized for individual nanorice by dark-field scattering spectroscopy. Compared with dipolar resonance, the line widths of high-order resonance peaks are narrower due to reduced radiative damping. As the length of the nanorice increases, these longitudinal LSPR peaks are red-shifted. The shifting rates are reduced as the resonance order increases. A perfect spheroid 500-nm long and 60-nm wide was used as a model to simulate excited LSPRs [Fig. 3(c)] in order to understand better the multiple LSPRs in nanorice structures. The simulation results indicate that the nanorice has five distinct longitudinal resonances in the extinction spectrum, corresponding to the first five multipolar modes [Fig. 3(d)]. The transverse modes and the fourth and fifth order longitudinal modes are zoomed in, as shown in the left and right inset, respectively, in Fig. 3(d). The electric field distributions simulated under different incident wavelengths and angles are shown in Fig. 3(e). Quasi-standing-wave patterns are observed along the long axis. When the incident polarization aligns along the nanorice's long axis, only odd order longitudinal modes can be excited due to symmetry. When the incident polarization is oblique, all resonance modes can be excited efficiently. The polarization-dependent extinction properties of nanorice can be observed in an aligned nanorice array formed by stretching a polymer film with embedded nanorice [43]. After stretching the polymer film, embedded nanorice preferentially orient their long axes parallel with the stretching direction to assemble an aligned array. The LSPRs of the ensemble-aligned nanorice array are dependent on the polarization of incident light. For example, the intensity of longitudinal LSPRs in the stretched film is much stronger under parallel excitation (the incident beam polarized parallel to the stretching direction) than that under perpendicular excitation.

Electron energy loss spectroscopy (EELS) is an ideal technique for investigating the plasmonic features of metal nanostructures, because it can provide high resolution in both space and energy. EELS was used to observe the real-space distribution of the multipolar plasmon resonances in individual nanorice structures [41]. In these measurements, the specimen was put in the TEM system. When the incident electron beam passes through or near the specimen, fast electrons will transfer their kinetic energy to the specimen, and the plasmon oscillations are excited impulsively. By acquiring the change in electron energy, the plasmonic features can be revealed. Figure 4(a) shows an annular dark field (ADF) image of a silver nanorice (top) and a series of EELS spectra (bottom) collected at different positions. The probed position of each EELS spectrum is enclosed by a rectangle with the same color as that of the spectrum. Both transverse and multipolar longitudinal plasmon resonances are acquired in the EELS spectra. The spectral features vary with the shift of the probed position. To confirm the orders of these modes, a series of energy-filtered maps were extracted by selectively filtering the scattering energy belonging to each peak in the summed EELS spectra, as shown in Fig. 4(b). Standing-wave patterns in the intensity across the long axis of the nanorice were observed. Successive mode orders of longitudinal resonances can be distinguished by increasing energy loss. The transverse surface plasmon resonance is also resolved, which is strongly confined to the nanorice's surface. Comparing these observations of nanorice structures with that of silver nanorods having the same length, we can conclude that the non-uniform short-axis radius of nanorice leads to the shift of resonance energy, although the general plasmonic behavior is qualitatively similar to that of purely cylindrical nanorods.

2.3 Silver nanorice for plasmonic sensing

The longitudinal LSPRs of quasi-one-dimensional nanos-

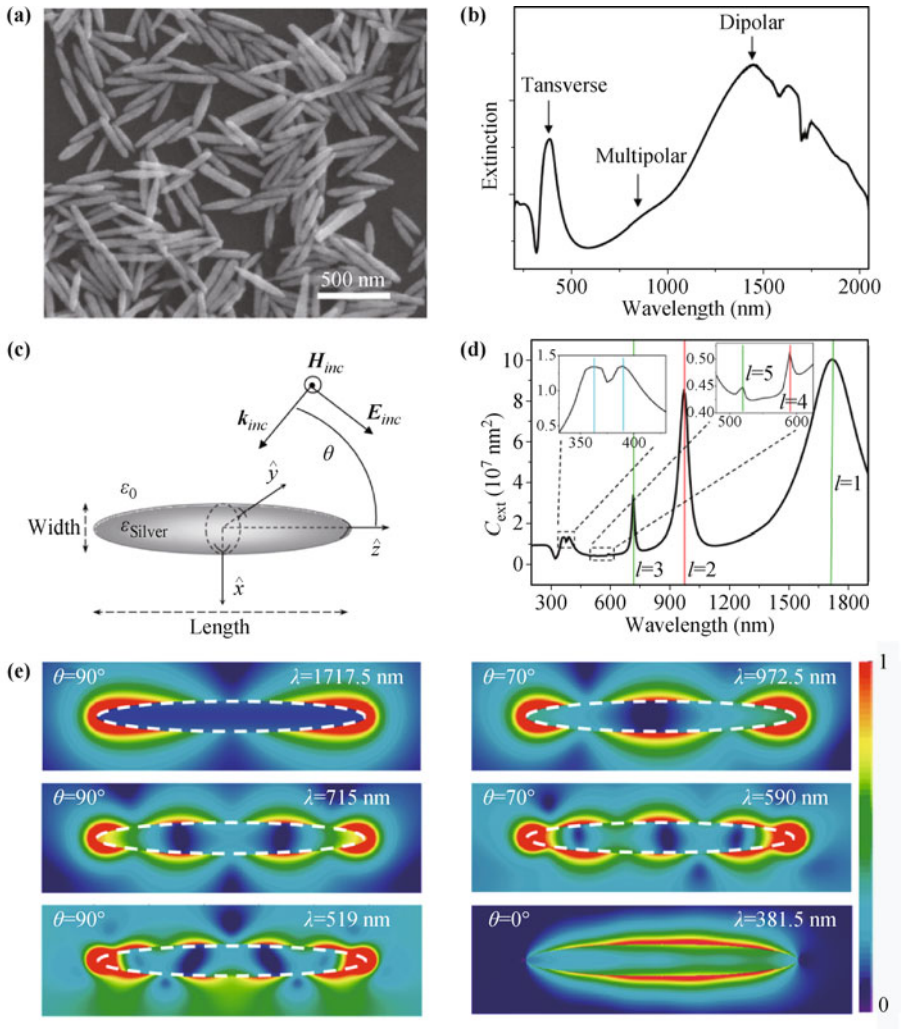

Fig. 3 **(a)** SEM image and **(b)** ensemble extinction spectrum of silver nanorice. **(c)** Model of nanorice used in simulations. **(d)** Simulated extinction cross section for a nanorice of 500 nm length and 60 nm width with an incident angle of 45°. The insets show the zoomed transverse (left) and 4th and 5th longitudinal (right) resonances. **(e)** Local electric field distributions in the x–z plane at the resonance wavelengths. Reproduced from Ref. [42].

tructures are highly sensitive to the surrounding media, which makes them ideal sensors for monitoring local environmental changes during biological or chemical processes [37, 38]. In such applications, two parameters are used to assess the actual performance of the sensors. One is the refractive index sensitivity, defined as the ratio between the shift of the resonance wavelength and the change of the refractive index (in unit of nm/RIU, RIU = refractive index unit), which provides a primary measure of sensor quality. Another is the figure of merit (FoM), defined as the refractive index sensitivity divided by the full width at half-maximum (FWHM) of the LSPR peak, which is a meaningful indicator for evaluating the sensor's performance [44]. Figure 5(a) shows the measurements of the LSPR sensitivities of nanorice structures for detecting changes in the surrounding dielectric media [41]. In our experiments, a monolayer of nanorice was deposited on a glass substrate and then immersed in different dielectric media to monitor the shifts of the resonance peaks. The results obtained from the extinction spectra of this nanorice sample show that both the transverse and the longitudinal plasmon resonance peaks red-shift linearly as the environmental refractive index increases, yet with quite different shift rates. The refractive index sensitivity of the longitudinal LSPR mode was 820.6 nm/RIU, remarkably higher than that of the transverse mode (47.3 nm/RIU). This result is even better than the calculated results for gold and silver nanorods [45]. The high sensitivity of the silver nanorice may result from their sharp apexes, larger aspect ratios, and lower resonance frequencies.

Recently, numerical calculations were carried out to study the performance of Fano-like interference of plasmon resonances in nanorice structures for refractometric

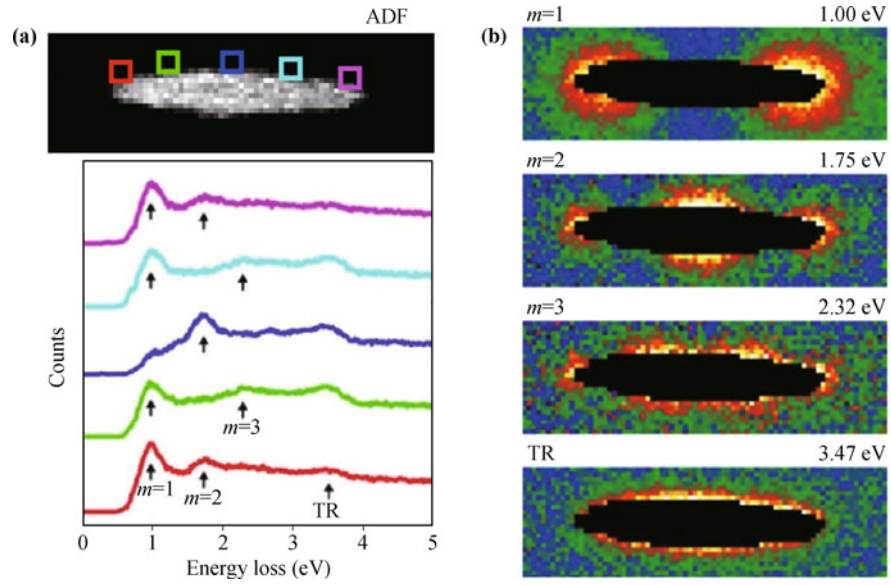

Fig. 4 **(a)** The EELS signals (after subtracting the zero loss peak) probed at different positions of a nanorice as marked on the top ADF image. **(b)** Intensity distributions mapped under different resonances energies. Reproduced from Ref. [41].

sensing under realistic conditions [44]. In the scattering spectra of individual silver nanorice, a narrow, asymmetric peak appears, as shown in Fig. 5(b). This asymmetric peak is explained as a result of Fano-like interference between adjacent plasmon resonances. In addition, when two nanorice of different size are arranged parallel to form a hetero dimer, distinctive multipolar Fano resonances are obtained under different illuminations based on a theoretical investigation [46]. For refractive index sensing, Fano-like plasmon resonance shows a great advantage. Due to the high sensitivity and narrow FWHM, a remarkably high FoM can be obtained [44]. Although the size dispersity in synthesized colloidal nanorice leads to peak broadening, a FoM with a value larger than 10 can still be obtained within a 5% size uncertainty [44].

The refractive index sensitivity of high-order plasmon resonances in a nanorice structure consisting of a silver core surrounded by an Al_2O_3 shell was investigated by numerical simulations [47]. The high-order resonances have narrower linewidths and larger quality factors, which are desired for sensing applications. With the increase of the dielectric shell thickness, the LSPR peak positions are red-shifted exponentially due to the exponential decay of the electromagnetic field intensity in the direction perpendicular to the Ag-Al_2O_3 interface.

Excitation of the LSPRs produces strong electric field at the surface of plasmonic nanostructures, as mentioned previously. If there are chemical species located nearby, the strong electric field can interact with them, and amplify many weak optical processes, such as surface-enhanced spectroscopy. Nanorods have been widely used in this field due to their tunable longitudinal LSPRs and huge electric field enhancements [48]. In nanorice structures, the intensity of the electric field increases in the vicinity of the elliptical ends, which benefits these types of applications. Wei *et al.* applied silver nanorice structures to SERS, and a significant enhancement was obtained [42]. Li *et al.* combined silver nanorice antennas with a patterned gold triangle nanoarray chip to create spatially broadened plasmonic "hot spots", which makes the composite structure an ultrasensitive SERS sensor [49].

3 Silver nanocarrot structures

3.1 Synthesis and structure characterization

Another asymmetric quasi-one-dimensional nanostructure is the silver nanocarrot, which was produced recently [40]. In a typical synthesis, 0.4 mL of 1M aqueous solution of CF_3COOAg and 0.222 g PVP, with an average molecular weight of 40 000, were added to 20 mL PEG 600 in a flask. The flask was heated at 95 °C in an oil bath for ∼18 h with continuous stirring. This synthesis process is similar to the one used for the synthesis of silver nanorice. The main difference is that the precursor used here is CF_3COOAg instead of $AgNO_3$. The carrot-like shape, with a tapered tail and a thicker head, is shown in the TEM image in Fig. 6(a). In order to reveal further the three-dimensional structure, tilted SEM measurements, as well as TEM thickness measurements, on individual nanocarrots were performed. The results show that the nanocarrot has a conical shape. A

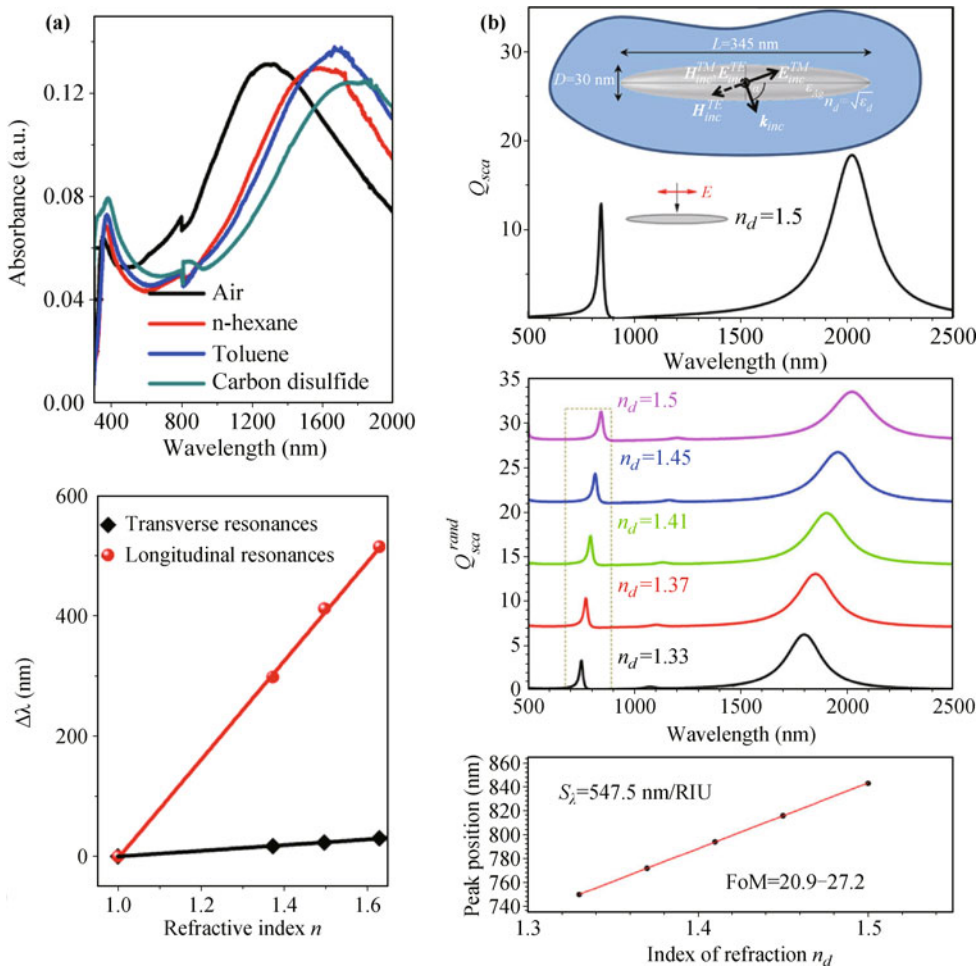

Fig. 5 **(a)** Top: Extinction spectra of a monolayer silver nanorice film on glass substrate immersed in different dielectric media; Down: The relationship between the peak shifts and the refractive index change. Reproduced from Ref. [41]. **(b)** Top: Calculated scattering efficiency of a silver nanorice in a medium of refractive index 1.5 with incident field polarized parallel to the long axis; Middle: Calculated scattering efficiencies for a nanorice of random orientation in the media of different refractive index; Down: Linear scaling of the peak positions inside the dashed box (middle panel) as a function of refractive index. Reproduced from Ref. [44].

detailed crystalline characterization was performed with HRTEM, XRD, and ED, as shown in Fig. 6. Similar to the crystalline structures of nanorice, the nanocarrot consists of mixed twins and stacking fault domains along the ⟨111⟩ direction of FCC phase, and a small amount of HCP phase. Further investigation indicates that the growth mechanism is also analogous to that of nanorice: elongated growth via oriented attachment combined with lateral growth by deposition of diffused metal atoms. The main difference is that during the oriented attachment process, relatively large seeds cap one end of the nanocarrot to terminate the longitudinal growth and stimulate lateral growth, which eventually leads to the formation of a big head and a tapered tail.

3.2 Plasmonic properties of nanocarrot structures

The plasmonic properties of nanocarrots were studied by both experiment and simulation, as shown in Fig. 7. Multipolar longitudinal modes were revealed clearly by the EELS spectrum of an individual particle and the extinction spectrum of a colloid suspension [top panel in Fig. 7(a)]. As the order of resonance increases, the peak amplitude decreases. Compared with the EELS spectrum of single nanocarrot, the ensemble extinction spectrum is broad because of the size/shape polydispersity. The EELS signals for nanocarrots depend strongly on the detection positions [lower panel in Fig. 7(a)], similar to what we saw for nanorice. For example, when the electron beam is focused on the terminals, the first order longitudinal mode ($m = 1$) is effectively excited, whereas when the electron beam is positioned in the middle, the first order resonance has a lower intensity, and the other three higher order successive modes (m= 2, 3, 4) appear. Under closer inspection, some subtle differences in

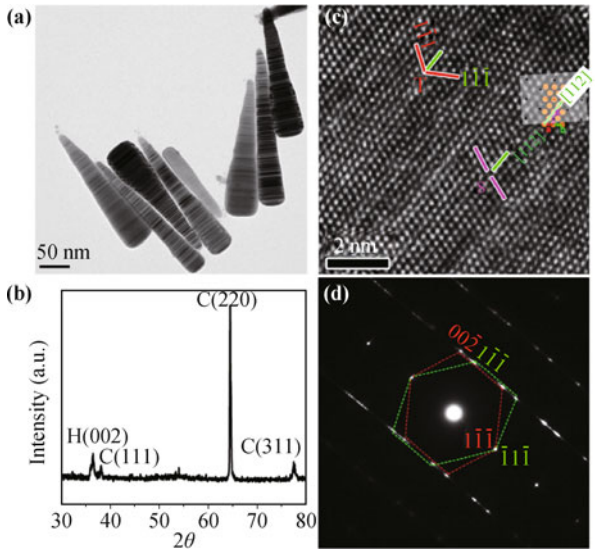

Fig. 6 **(a)** TEM image and **(b)** XRD pattern of silver nanocarrots. **(c)** HRTEM image and **(d)** corresponding ED pattern taken from the center part of a nanocarrot. In (c), twins and stacking faults are labeled as T and S, respectively. Reproduced from Ref. [40].

the plasmonic responses at the two terminals are apparent. With excitation at the tail (spectrum 1, black line), the peak intensity of the $m = 1$ mode is amplified. With excitation at the head (spectrum 5, purple line), the peak intensity of the $m = 1$ mode is lower and the $m = 4$ mode disappears. These differences between the excitations at the two terminals are attributed to varying diameters and curvatures. A series of energy-filtered maps in Fig. 7(b) further reveal the spatial characteristics of LSPRs belonging to each order of resonance. The standing-wave patterns in the EELS maps are explained by the interference of counter-propagating surface plasmons. These maps resemble that of nanorod structures, which can be regarded as FP resonances along the long axis. However, the distribution of the nodes along the axis of the nanocarrot shows clear asymmetry [40].

In order to compare the plasmonic responses of an asymmetric silver nanocarrot with a symmetric silver nanorod, their EELS maps were measured, as shown in Fig. 8(a). The asymmetric electric field distributions in the nanocarrot are noticeable, and the distance between adjacent nodes decreases as we go toward the tail of the nanocarrot. This result is reproduced by simulation [Fig. 8(b)], which further proves that the asymmetric plasmonic response of the nanocarrot results from its

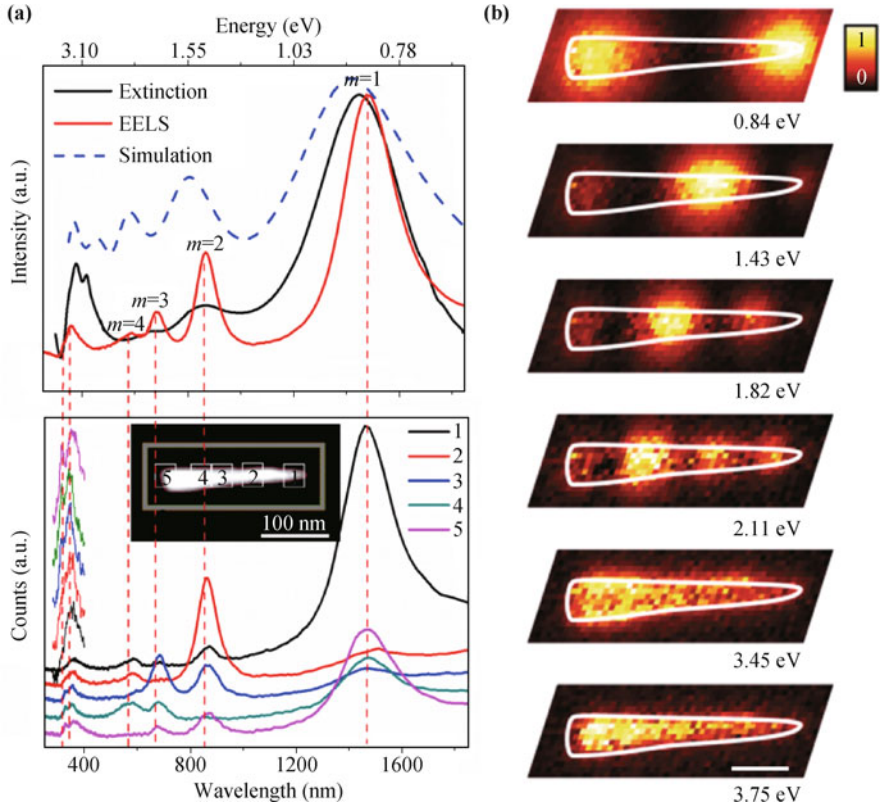

Fig. 7 **(a)** Top: Optical extinction spectrum of the nanocarrot ensemble (*black*), EELS spectrum (*red*) and simulated optical extinction spectrum (*blue*) of an individual nanocarrot; Down: EELS signals acquired at five different positions as marked on the ADF image in the inset. The transverse peaks are enlarged and vertically offset to improve the readability. The dashed lines are guides to the eye joining identical resonance modes. **(b)** EELS maps of multiple plasmon resonances. The scale bar is 50 nm. Reproduced from Ref. [40].

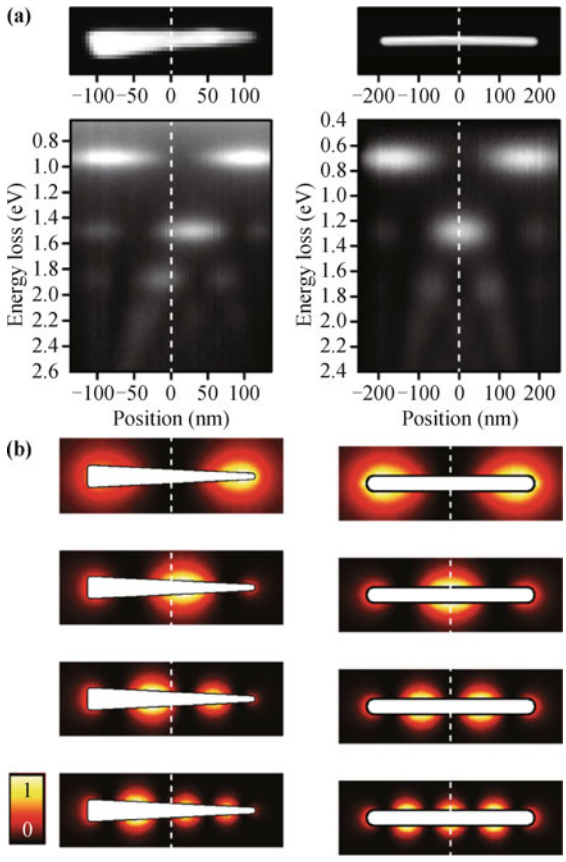

Fig. 8 **(a)** Comparison of the plasmonic responses of an asymmetric silver nanocarrot (left) and a symmetric silver nanorod (right) using EELS mapping. **(b)** Calculated maps of electron energy loss probability for a nanocarrot (left) and a nanorod (right) with same length. Reproduced from Ref. [40].

asymmetric structure. This phenomenon may be caused by variations in the velocity of the surface plasmon polaritons (SPPs). The thinner tip in a nanocarrot can be considered as a cylinder with a smaller diameter, where the SPPs are more localized and their propagations are slower than propagations at the broader head. Finally, the slower SPPs lead to the nodes toward the tail.

Similar to nanorods [34], the longitudinal LSPRs in nanocarrots depend on the aspect ratio. By changing the aspect ratio of the nanocarrot, the longitudinal resonances can be tuned accordingly. Both experimental and theoretical analyses show that the longitudinal resonance peaks red-shift linearly with increasing nanocarrot length. By keeping the width nearly constant, the shift is more obvious for lower-order resonances [40]. Moreover, the plasmonic properties of nanocarrots also depend on the polarization of incident light. In stretched polymer films, the embedded nanocarrots are aligned with the long axes preferably oriented along the stretched direction. The longitudinal resonances can only be efficiently excited when the incident light is polarized parallel to the long axes [43].

3.3 Silver nanocarrot for plasmonic sensing

LSPRs in silver nanocarrots are also highly sensitive to changes in the surrounding dielectric media. Their performance for refractive index sensing was evaluated by dispersing them in a mixture of ethanol and PEG 600 with various volume ratios to measure the shifts of their resonance peaks. A high refractive index sensitivity of 890 ± 87 nm/RIU was obtained for the first order longitudinal mode, which resulted from the sharp tip and the large aspect ratio. Such high sensitivity makes them very attractive for sensing applications. Moreover, experimental and simulation results show that the localization of SPPs around the taper tip of the nanocarrot can produce a higher field enhancement because of so-called "self-focusing", or lighting rod effect [40]. This advantage makes them ideal for applications utilizing the field enhancement effect, such as surface-enhanced spectroscopy.

4 Conclusions

In conclusion, we reviewed the syntheses and investigations of the plasmonic features of silver nanorice and silver nanocarrot, two silver nanostructures with shapes deviating from cylindrical nanorods. These two quasi-one-dimensional nanostructures have optical properties similar to nanorods. Both of them support transverse and multipolar longitudinal LSPRs. The latter ones are analogous to FP resonances. The resonance peaks of the longitudinal modes red-shift linearly with increasing aspect ratio. Their electric field distributions show standing-wave patterns along the long axis, as shown in the EELS maps and the simulation results. In addition, Fano-like interference occurs in nanorice, due to the interaction between two adjacent modes. The shape deviation from a nanorod has some effects on the plasmonic properties. For example, different from a nanorod, the non-uniform short-axis radius of nanorice leads to the shift of resonance energy, and the sharp tip generates a strong electric field. In nanocarrot structures, the asymmetric shape causes the compression of the charge distribution towards the tail and the localization of SPPs around the taper tip, which can produce higher field enhancement because of the "self-focusing" phenomenon. These investigations provide a deep understanding of the shape-dependent plasmonic properties that can potentially be used in sensing, surface-enhanced spectroscopy, and other applications.

Acknowledgements This work was supported by the Ministry of Science and Technology of China (Grant Nos. 2012YQ12006005 and 2015CB932400), the National Natural Science Foundation of

China (Grant Nos. 11134013, 11227407, 11374012, and 11422436), and the "Strategic Priority Research Program (B)" of Chinese Academy of Sciences (Grant No. XDB07030100).

References

1. W. A. Murray and W. L. Barnes, Plasmonic materials, *Adv. Mater.* 19(22), 3771 (2007)
2. H. Wei and H. X. Xu, Plasmonics in composite nanostructures, *Mater. Today* 17(8), 372 (2014)
3. L. M. Tong, H. Wei, S. P. Zhang, Z. P. Li, and H. X. Xu, Optical properties of single coupled plasmonic nanoparticles, *Phys. Chem. Chem. Phys.* 15(12), 4100 (2013)
4. L. M. Tong and H. X. Xu, Frontiers of plasmonics, *Front. Phys.* 9(1), 1 (2014)
5. O. Stranik, J. Jatschka, A. Csakiand, and W. Fritzsche, Development of new classes of plasmon active nano-structures and their application in bio-sensing and energy guiding, *Front. Phys.* 9(5), 652 (2014)
6. K. M. Mayer and J. H. Hafner, Localized surface plasmon resonance sensors, *Chem. Rev.* 111(6), 3828 (2011)
7. H. X. Xu, E. J. Bjerneld, M. Kall, and L. Borjesson, Spectroscopy of single hemoglobin molecules by surface enhanced Raman scattering, *Phys. Rev. Lett.* 83(21), 4357 (1999)
8. H. X. Xu, J. Aizpurua, M. Kall, and P. Apell, Electromagnetic contributions to single-molecule sensitivity in surface-enhanced Raman scattering, *Phys. Rev. E* 62, 4318 (2000)
9. H. Y. Liang, Z. P. Li, W. Z. Wang, Y. S. Wu, and H. X. Xu, Highly surface-roughened "flower-like" silver nanoparticles for extremely sensitive substrates of surface-enhanced Raman scattering, *Adv. Mater.* 21(45), 4614 (2009)
10. H. Y. Liang, Z. P. Li, Z. X. Wang, W. Z. Wang, F. Rosei, D. L. Ma, and H. X. Xu, Enormous surface-enhanced Raman scattering from dimers of flower-like silver mesoparticles, *Small* 8(22), 3400 (2012)
11. H. X. Xu, Theoretical study of coated spherical metallic nanoparticles for single-molecule surface-enhanced spectroscopy, *Appl. Phys. Lett.* 85(24), 5980 (2004)
12. H. Wei and H. X. Xu, Hot spots in different metal nanostructures for plasmon-enhanced Raman spectroscopy, *Nanoscale* 5(22), 10794 (2013)
13. A. M. Michaels, J. Jiang, and L. Brus, Ag nanocrystal junctions as the site for surface-enhanced Raman scattering of single Rhodamine 6G molecules, *J. Phys. Chem. B* 104(50), 11965 (2000)
14. M. Moskovits, Surface-enhanced Raman spectroscopy: A brief retrospective, *J. Raman Spectrosc.* 36(6–7), 485 (2005)
15. J. F. Li, Y. F. Huang, Y. Ding, Z. L. Yang, S. B. Li, X. S. Zhou, F. R. Fan, W. Zhang, Z. Y. Zhou, Y. Wu, B. Ren, Z. L. Wang, and Z. Q. Tian, Shell-isolated nanoparticle-enhanced Raman spectroscopy, *Nature* 464(7287), 392 (2010)
16. F. Z. Cong, H. Wei, X. R. Tian, and H. X. Xu, A facile synthesis of branched silver nanowire structures and its applications in surface-enhanced Raman scattering, *Front. Phys.* 7(5), 521 (2012)
17. Z. H. Kim, Single-molecule surface-enhanced Raman scattering: Current status and future perspective, *Front. Phys.* 9(1), 25 (2014)
18. Y. S. Yamamoto, M. Ishikawa, Y. Ozaki, and T. Itoh, Fundamental studies on enhancement and blinking mechanism of surface-enhanced Raman scattering (SERS) and basic applications of SERS biological sensing, *Front. Phys.* 9(1), 31 (2014)
19. L. M. Tong, H. Wei, S. P. Zhang, and H. X. Xu, Recent advances in plasmonic sensors, *Sensors* 14(5), 7959 (2014)
20. H. X. Xu and M. Kall, Modeling the optical response of nanoparticle-based surface plasmon resonance sensors, *Sens. Actuators B Chem.* 87(2), 244 (2002)
21. H. X. Xu and M. Käll, Surface-plasmon-enhanced optical forces in silver nanoaggregates, *Phys. Rev. Lett.* 89(24), 246802 (2002)
22. F. Svedberg, Z. P. Li, H. X. Xu, and M. Käll, Creating hot nanoparticle pairs for surface-enhanced Raman spectroscopy through optical manipulation, *Nano Lett.* 6(12), 2639 (2006)
23. M. L. Juan, M. Righini, and R. Quidant, Plasmon nano-optical tweezers, *Nat. Photonics* 5(6), 349 (2011)
24. T. Shegai, Z. P. Li, T. Dadosh, Z. Y. Zhang, H. X. Xu, and G. Haran, Managing light polarization via plasmon-molecule interactions within an asymmetric metal nanoparticle trimer, *Proc. Natl. Acad. Sci. USA* 105(43), 16448 (2008)
25. V. Giannini, A. I. Fernández-Domínguez, S. C. Heck, and S. A. Maier, Plasmonic nanoantennas: fundamentals and their use in controlling the radiative properties of nanoemitters, *Chem. Rev.* 111(6), 3888 (2011)
26. Z. P. Li, T. Shegai, G. Haran, and H. X. Xu, Multiple-particle nanoantennas for enormous enhancement and polarization control of light emission, *ACS Nano* 3(3), 637 (2009)
27. B. S. Guiton, V. Iberi, S. Li, D. N. Leonard, C. M. Parish, P. G. Kotula, M. Varela, G. C. Schatz, S. J. Pennycook, and J. P. Camden, Correlated optical measurements and plasmon mapping of silver nanorods, *Nano Lett.* 11(8), 3482 (2011)
28. A. L. Schmucker, N. Harris, M. J. Banholzer, M. G. Blaber, K. D. Osberg, G. C. Schatz, and C. A. Mirkin, Correlating nanorod structure with experimentally measured and theoretically predicted surface plasmon resonance, *ACS Nano* 4(9), 5453 (2010)
29. S. P. Zhang, L. Chen, Y. Z. Huang, and H. X. Xu, Reduced linewidth multipolar plasmon resonances in metal nanorods and related applications, *Nanoscale* 5(15), 6985 (2013)
30. S. Link and M. A. El-Sayed, Spectral properties and relaxation dynamics of surface plasmon electronic oscillations in

gold and silver nanodots and nanorods, *J. Phys. Chem. B* 103(40), 8410 (1999)

31. L. Vigderman, B. P. Khanal, and E. R. Zubarev, Functional gold nanorods: Synthesis, self-assembly, and sensing applications., *Adv. Mater.* 24(36), 4811, 5014 (2012)
32. J. Aizpurua, G. W. Bryant, L. J. Richter, F. J. G. de Abajo, B. K. Kelley, and T. Mallouk, Optical properties of coupled metallic nanorods for field-enhanced spectroscopy, *Phys. Rev. B* 71(23), 235420 (2005)
33. M. B. Mohamed, V. Volkov, S. Link, and M. A. El-Sayed, The "lightning" gold nanorods: Fluorescence enhancement of over a million compared to the gold metal, *Chem. Phys. Lett.* 317(6), 517 (2000)
34. G. W. Bryant, F. J. García de Abajo, and J. Aizpurua, Mapping the plasmon resonances of metallic nanoantennas, *Nano Lett.* 8(2), 631 (2008)
35. H. Y. Liang, W. Z. Wang, Y. Z. Huang, S. P. Zhang, H. Wei, and H. X. Xu, Controlled synthesis of uniform silver nanospheres, *J. Phys. Chem. C* 114(16), 7427 (2010)
36. D. Rossouw and G. A. Botton, Resonant optical excitations in complementary plasmonic nanostructures, *Opt. Express* 20(7), 6968 (2012)
37. A. V. Kabashin, P. Evans, S. Pastkovsky, W. Hendren, G. A. Wurtz, R. Atkinson, R. Pollard, V. A. Podolskiy, and A. V. Zayats, Plasmonic nanorod metamaterials for biosensing, *Nat. Mater.* 8(11), 867 (2009)
38. P. Zijlstra, P. M. R. Paulo, and M. Orrit, Optical detection of single non-absorbing molecules using the surface plasmon resonance of a gold nanorod, *Nat. Nanotechnol.* 7(6), 379 (2012)
39. H. Y. Liang, H. X. Yang, W. Z. Wang, J. Q. Li, and H. X. Xu, High-yield uniform synthesis and microstructure-determination of rice-shaped silver nanocrystals, *J. Am. Chem. Soc.* 131(17), 6068 (2009)
40. H. Y. Liang, D. Rossouw, H. G. Zhao, S. K. Cushing, H. L. Shi, A. Korinek, H. X. Xu, F. Rosei, W. Z. Wang, N. Q. Wu, G. A. Botton, and D. L. Ma, Asymmetric silver "nanocarrot" structures: Solution synthesis and their asymmetric plasmonic resonances, *J. Am. Chem. Soc.* 135(26), 9616 (2013)
41. H. Y. Liang, H. G. Zhao, D. Rossouw, W. Z. Wang, H. X. Xu, G. A. Botton, and D. L. Ma, Silver nanorice structures: Oriented attachment-dominated growth, high environmental sensitivity, and real-space visualization of multipolar resonances, *Chem. Mater.* 24(12), 2339 (2012)
42. H. Wei, A. Reyes-Coronado, P. Nordlander, J. Aizpurua, and H. X. Xu, Multipolar plasmon resonances in individual Ag nanorice, *ACS Nano* 4(5), 2649 (2010)
43. X. Tong, H. Y. Liang, Y. L. Liu, L. Tan, D. L. Ma, and Y. Zhao, Anisotropic optical properties of oriented silver nanorice and nanocarrots in stretched polymer films, *Nanoscale* 7(19), 8858 (2015)
44. F. López-Tejeira, R. Paniagua-Domínguez, and J. A. Sánchez-Gil, High-performance nanosensors based on plasmonic Fano-like interference: Probing refractive index with individual nanorice and nanobelts, *ACS Nano* 6(10), 8989 (2012)
45. J. S. Sekhon and S. S. Verma, Refractive index sensitivity analysis of Ag, Au, and Cu nanoparticles, *Plasmonics* 6(2), 311 (2011)
46. X. R. Tian, Y. R. Fang, and B. L. Zhang, Multipolar Fano resonances and Fano-assisted optical activity in silver nanorice heterodimers, *ACS Photonics* 1(11), 1156 (2014)
47. L. Chen, H. Wei, K. Q. Chen, and H. X. Xu, High-order plasmon resonances in an Ag/Al_2O_3 core/shell nanorice, *Chin. Phys. B* 23(2), 027303 (2014)
48. S. Shanmukh, L. Jones, J. Driskell, Y. P. Zhao, R. Dluhy, and R. A. Tripp, Rapid and sensitive detection of respiratory virus molecular signatures using a silver nanorod array SERS substrate, *Nano Lett.* 6(11), 2630 (2006)
49. M. Li, S. K. Cushing, H. Y. Liang, S. Suri, D. L. Ma, and N. Q. Wu, Plasmonic nanorice antenna on triangle nanoarray for surface-enhanced Raman scattering detection of hepatitis B virus DNA, *Anal. Chem.* 85(4), 2072 (2013)